AIP | Review of Scientific Instruments

High-stability cryogenic scanning tunneling microscope based on a closed-cycle cryostat

Jason D. Hackley, Dmitry A. Kislitsyn, Daniel K. Beaman, Stefan Ulrich, and George V. Nazin

Citation: Review of Scientific Instruments **85**, 103704 (2014); doi: 10.1063/1.4897139
View online: http://dx.doi.org/10.1063/1.4897139
View Table of Contents: http://scitation.aip.org/content/aip/journal/rsi/85/10?ver=pdfcov
Published by the AIP Publishing

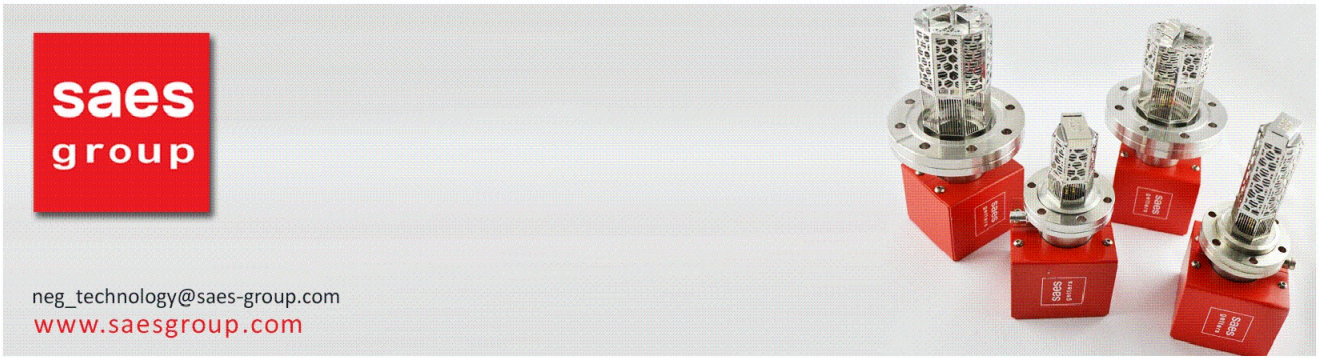

High-stability cryogenic scanning tunneling microscope based on a closed-cycle cryostat

Jason D. Hackley,[1] Dmitry A. Kislitsyn,[1] Daniel K. Beaman,[1,a)] Stefan Ulrich,[2] and George V. Nazin[1,b)]
[1]*Department of Chemistry and Biochemistry, 1253 University of Oregon, Eugene, Oregon 97403, USA*
[2]*RHK Technology, Inc., 1050 East Maple Road, Troy, Michigan 48083, USA*

(Received 4 June 2014; accepted 21 September 2014; published online 7 October 2014)

We report on the design and operation of a cryogenic ultra-high vacuum (UHV) scanning tunneling microscope (STM) coupled to a closed-cycle cryostat (CCC). The STM is thermally linked to the CCC through helium exchange gas confined inside a volume enclosed by highly flexible rubber bellows. The STM is thus mechanically decoupled from the CCC, which results in a significant reduction of the mechanical noise transferred from the CCC to the STM. Noise analysis of the tunneling current shows current fluctuations up to 4% of the total current, which translates into tip-sample distance variations of up to 1.5 picometers. This noise level is sufficiently low for atomic-resolution imaging of a wide variety of surfaces. To demonstrate this, atomic-resolution images of Au(111) and NaCl(100)/Au(111) surfaces, as well as of carbon nanotubes deposited on Au(111), were obtained. Thermal drift analysis showed that under optimized conditions, the lateral stability of the STM scanner can be as low as 0.18 Å/h. Scanning Tunneling Spectroscopy measurements based on the lock-in technique were also carried out, and showed no detectable presence of noise from the closed-cycle cryostat. Using this cooling approach, temperatures as low as 16 K at the STM scanner have been achieved, with the complete cool-down of the system typically taking up to 12 h. These results demonstrate that the constructed CCC-coupled STM is a highly stable instrument capable of highly detailed spectroscopic investigations of materials and surfaces at the atomic scale. [http://dx.doi.org/10.1063/1.4897139]

I. INTRODUCTION

Now in its fourth decade of existence, scanning tunneling microscopy (STM)[1] has become an essential tool that has provided unique insights into the atomic structures of a wide variety of surfaces and nanoscale systems. Scanning Tunneling Spectroscopy (STS)[1] is one of the important capabilities of STM that provides atomic-resolution information about the electronic structures of sample surfaces. STM experiments probing the spatially dependent spectroscopic properties of surfaces at the atomic scale typically require ultra high vacuum (UHV) conditions and cryogenic temperatures: UHV enables preparation and use of well-defined atomically clean surfaces, while low-temperatures greatly enhance the mechanical stability of the STM junction, freeze the motion of weakly bound adsorbates, and improve the spectroscopic resolution of STS by reducing the thermal broadening of spectroscopic features. The majority of STM systems intended for high-performance STS experiments have so far been constructed coupled to a variety of different cryostats, such as continuous-flow[2–4] or bath-cryostats.[5–7] So far, operation of all of these cryostats has relied on the use of cryogens, with the best operating conditions achievable with liquid helium. The dramatic increase of liquid helium costs over the past decade[8] has led to a situation where using liquid-helium for STM instruments is becoming prohibitively expensive for research groups without access to a helium liquefier. Near-future projections predict further price increases of up to 50%.[8] Development of a cryogen-free STM operating at near liquid-helium temperatures is thus important for sustaining the current level of activity of STS-based studies in a variety of research fields.

In this communication, we present a novel cryogenic UHV-STM instrument that, for the first time, achieves temperatures as low as 16 K by using a closed-cycle cryostat (CCC).[9] The cryostat is based on the Gifford-McMahon (GM) design, which uses recirculating helium-gas thus obviating the need for liquid helium. The use of a CCC for STM is counterintuitive due to the inherent noise of CCCs: GM cold-heads, in particular, incorporate moving parts located in close proximity of the cold finger where instrumentation is typically mounted. Another variation of CCC, pulse-tube based refrigerators, also displays significant mechanical vibrations.[10] By using a novel CCC, which is thermally linked to the STM system through helium exchange gas inside a volume confined by highly flexible rubber bellows, we have achieved a significant reduction of the mechanical noise transferred from the CCC to the STM.

The performance of the new STM is comparable to the established designs based on the continuous flow- or bath-cryostats. Noise analysis of the tunneling current shows current fluctuations up to 4% of the total current, which translates into tip-sample distance variations of up to 1.5 picometers. This noise level is sufficiently low to allow atomic-resolution imaging of most surfaces typically studied with STM, as

a)Present address: Intel Corporation, Hillsboro, Oregon 97124, USA.
b)Author to whom correspondence should be addressed. Electronic mail: gnazin@uoregon.edu

demonstrated in this paper using Au(111) and NaCl(100)/Au(111) surfaces, as well as carbon nanotubes deposited on Au(111). With the need for conservation of liquid helium removed, we are able to actively stabilize the temperature of the scanner using a heater controlled by a feedback mechanism. This enables temperature stability on the scale of ±1 milli-Kelvin (mK), which leads to extremely low lateral and vertical (tip-sample distance) drift rates. Thermal drift analysis showed that under optimized conditions, the lateral stability of the STM scanner can be as low as 0.18 Å/h. STS measurements (based on the lock-in technique) with the new STM show no detectable presence of noise from the closed-cycle cryostat.

II. SYSTEM DESIGN

A. STM/scan head

Despite the mechanical separation of the STM chamber from the CCC, residual mechanical noise appearing as spikes of up to 5 nm can still be present on the cryostat cold-finger mounted on the STM chamber side.[11] These vibrations have a low frequency of 2.4 Hz, which makes it imperative for the STM scanner assembly (including the sample and sample holder) to be as rigid as possible. The Pan-style design[6] was therefore chosen for the STM scanner, as it is one of the most rigid designs developed so far.[12]

The STM scanner, constructed by RHK Technology, incorporates a set of piezo-drive positioners, which, in addition to the coarse approach capability realized by a Pan-style Z-positioner, allow lateral coarse-positioning of the sample using a combined XY piezo-drive positioner.[13] The total range of all three positioners covers a volume of 8 mm × 4.5 mm × 4.5 mm. The positioners are assembled onto a rigid gold-plated molybdenum housing (Fig. 1). Molybdenum was chosen because in addition to high stiffness, it possesses good thermal conductivity and a low thermal expansion coefficient that is a good match for other components of the system. The body of the scanner was designed to accommodate an additional set of piezo motors for positioning of optics for Scanning Tunneling Luminescence experiments.[14–17] The constructed STM scanner is highly immune to external vibrations and is capable of atomic-resolution imaging (of graphite surfaces) in ambient conditions with minimal vibrational isolation (e.g., a rubber pad placed under the scanner was found to be sufficient). For optimal vibrational isolation, our STM is suspended on stainless steel springs, and is eddy-current damped by eight samarium-cobalt magnets attached to the STM body (Fig. 1). Each spring consists of two sections connected with a ceramic/stainless-steel coupler acting as an electrical and thermal break. The natural frequency of the hanging STM is 1.7 Hz, below the fundamental noise frequency generated by the CCC.

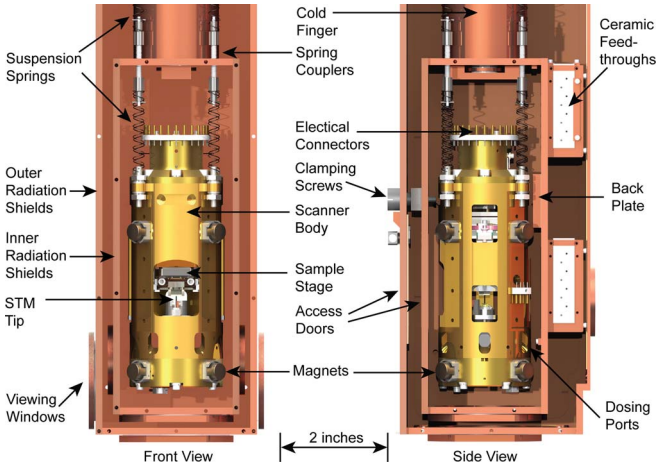

FIG. 1. STM scanner suspended inside the thermal radiation shields. Left: Front view of STM in shields with front-facing shields removed. Right: Side view of STM in shields with side-facing shields removed. The inner radiation shield is mounted directly to the cold tip, which is the second cooling stage of the cold finger. The outer radiation shields mount directly to the first cooling stage of the cold finger (not shown). Springs extend approximately four inches above the area shown.

B. Radiation shields

To achieve near-liquid helium temperatures, our design incorporates two nested thermal radiation shields constructed from gold-plated oxygen-free high-conductivity copper (Fig. 1).[3] The two radiation shields are mounted to two cooling stages of the CCC: the outer thermal shield is attached to the first cooling stage (not shown), which during experiment is at 25–35 K; and the inner radiation shield is attached to the second cooling stage (Cold Finger in Fig. 1), and is typically at ∼15 K. The target temperature is typically maintained a fraction of a degree above the minimal attainable temperature using a heater wound on the cold finger. The heater is regulated using the feedback control loop of the temperature controller.

The STM body is cooled via a bundle of fine copper wires (0.005 in.) connected to the top of the inner radiation shield via a sapphire piece (sapphire was chosen in order to avoid direct electrical contact). Additional cooling is provided by electrical connections (0.005 in. copper wires) connected to electrical feedthrough panels mounted on the backside of the inner shield (Fig. 1). The feedthrough panels were made from Shapal Hi-M Soft™,[18] which has high thermal conductivity thus providing efficient thermal anchoring of electrical connections to the inner shield. Electrical connections from the inner shield feedthrough panels to the outside were made using stainless steel wires to minimize the thermal leak. To minimize the thermal load on the feedthrough panels, the stainless steel wires are thermally anchored at the outer thermal shield. During cool down, two spring-loaded screws mounted on the inner radiation shield are used to clamp the STM scanner to the back plate of the inner radiation shield (Fig. 1). The screws are released upon reaching the target temperature, so that the STM scanner hangs free, with the scanner temperature about 1.3 K higher than that of the inner radiation shield.

Each radiation shield incorporates a set of windows (sapphire for the inner shield and fused silica for the outer shield), which allow fine-scale observation of the STM junction and sample, as well as monitoring tip or sample exchange. The radiation shields, as well as the STM scanner, were designed and constructed with line-of-site openings for

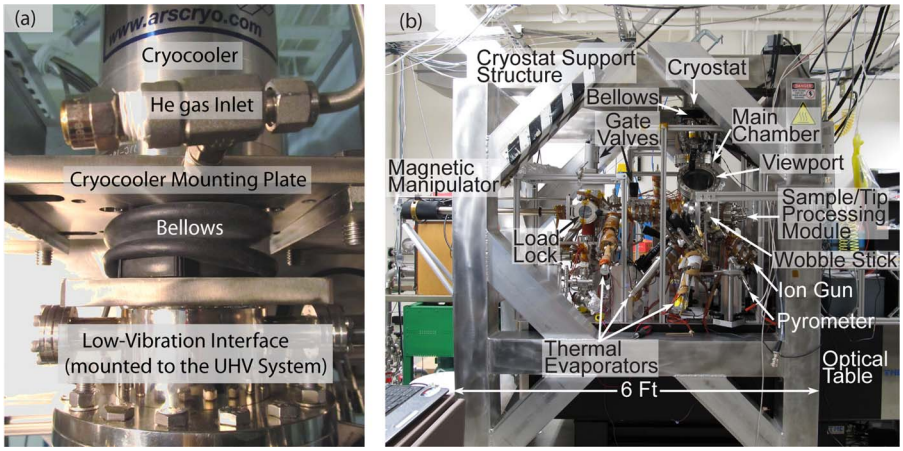

FIG. 2. Overview of the vacuum and cooling systems. (a) Thermal connection between the Cryocooler and Cold Finger is realized via the He-filled volume confined by a rubber bellows. (b) View of the UHV system. The cryostat is mounted to the cryostat support structure above the UHV system. The cryostat support structure has no contact with the UHV system.

in situ evaporation/dosing directly into the STM junction by using thermal evaporators or gas sources mounted in the UHV system.

C. Cooling system

To achieve cryogenic temperatures, we used a CCC manufactured by Advanced Research Systems, Inc.[9] The main components of the CCC are: (1) the GM cryocooler [DE202PF, Fig. 2(a)]; (2) a low-vibration interface (DMX-20) incorporating a UHV-compatible cold finger to which the STM radiation shields are mounted [Fig. 2(a)]; and (3) a water-cooled compressor (ARS-2HW, not shown) that supplies compressed helium to the cryocooler. The cryocooler, the main source of the 2.4 Hz noise, is mounted on a separate support structure that is mechanically decoupled from the STM system [Fig. 2(b)], and is anchored directly to the floor surface that is in direct contact with the underlying bedrock below the laboratory space. The thermal link between the cooler and cold finger is realized using a heat exchange interface consisting of a rubber bellows filled with helium gas, with the rubber bellows being the only source of mechanical coupling between the cryocooler and the UHV system. While this does not completely eliminate vibrations, the residual vibrational noise typically registered at the cold finger end is within 5 nm, four orders of magnitude lower than the noise level at the cryocooler.[11]

D. UHV system design

Several measures were taken to minimize the noise experienced by the STM system. The UHV STM system was assembled on the rigid concrete floor of the basement. The floor is anchored to the underlying bedrock via six reinforced concrete piers. The UHV chamber sits on an optical table with rigid mount legs without any additional vibrational isolation. The system is located in a "sound proof" room with low-noise ventilation baffles and dampers maintaining laminar air flow. The roughing pumps are located in an isolated pump room. The vacuum backing lines were attached to the chamber via stainless steel bellows, and are routed through sand-filled boxes to damp the mechanical vibrations generated by the backing pumps.

The vacuum system is composed of the main chamber, a load-lock chamber for quick tip and sample exchange, and a process gas manifold, each with a dedicated pumping line composed of a 75 L/s turbo pump and a dry scroll pump. In the case of the main chamber, the 75 L/s turbo pump serves as a backing pump for a 300 L/s magnetically levitated turbo pump mounted directly on the chamber. In addition, the main chamber is pumped by a 300 L/s ion pump integrated with a combination of a titanium sublimation pump and a cryogenically cooled shroud. The baseline pressure in the main chamber is $\sim 4 \times 10^{-11}$ Torr, and at 2×10^{-11} Torr during experiments at cryogenic temperatures, due to the cryo-pumping action of the radiation shields/cryostat.

E. Sample preparation

In addition to the STM, the main chamber houses tip- and sample preparation and storage facilities. Samples (mounted on molybdenum sample holders) and tips are stored in a "carousel" module inside the main chamber (Fig. 3) with nine slots for samples and thirty slots for tips. The samples and tips are exchanged between the load lock and the main UHV chamber by using a precision magnetic manipulator. Inside the main chamber, the samples and tips are manipulated using a wobble-stick allowing three-dimensional translation and rotation around the wobble-stick axis. Tips and samples are prepared *in situ* via cycles of annealing and neon-ion-sputtering using a custom multifunctional processing module (Fig. 3). The module incorporates a current-carrying filament that can either be used for e-beam or radiation heating of individual samples and tips.[3] During the annealing process, the temperature of the sample is monitored by a pyrometer. An ion gun is used for sample sputtering, while tips are self-sputtered when biased to high voltage in neon pressure.

After an atomically clean sample surface is obtained, a wide variety of materials can be deposited on the sur-

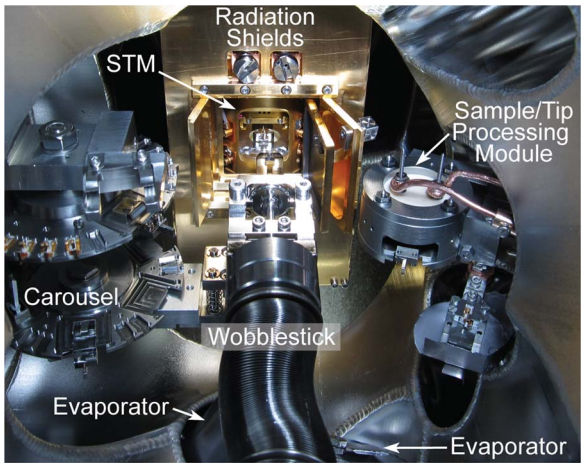

FIG. 3. View of the main chamber interior looking through the view port. Both the outer and inner radiation shield doors are open, affording a view of the STM.

face using several facilities implemented in the system. Four different ports are available on the main chamber for mounting either gas/vapor sources or thermal evaporators [Fig. 2(b)], two of which are aligned into the STM junction. Thus, materials with appropriate vapor pressures can be evaporated *in situ*. All of these ports have dedicated gate valves, which allow exchange of gas/vapor sources or thermal evaporators without breaking vacuum in the main chamber. A "dry contact transfer"[19] capability is available for deposition of nanoscale and molecular materials that do not have sufficient vapor pressures for evaporation, such as carbon nanotubes, graphene flakes, and polymers. A facility for deposition of materials from solution using a pulsed valve[20,21] is implemented in the load-lock, and has been successfully used for deposition of colloidal quantum dots.

III. PERFORMANCE

A. Cool-down and operation

Full cool-down of the STM from room temperature to near-liquid helium temperatures takes approximately 12 h [Fig. 4(a)], and is typically carried out overnight. During cool down, the STM is clamped to the back plate of the inner radiation shield. Upon reaching the target temperature the STM is unclamped and hangs free. After the cool-down, the cold-finger temperature is actively stabilized using a heater controlled by a feedback mechanism, such that the STM temperature remains stable for days within ±1 mK [Fig. 4(b)]. The high temperature stability enables extremely low lateral and vertical tip-sample drift rates, as described below. So far, we have found no limitation on the duration of individual experiments: we have conducted experiments lasting several weeks without any major changes in operating conditions, except for the need to periodically (every several days) to increase the feedback set-point temperature. This is likely due to condensation of air/water vapor inside the volume filled with exchange He gas.

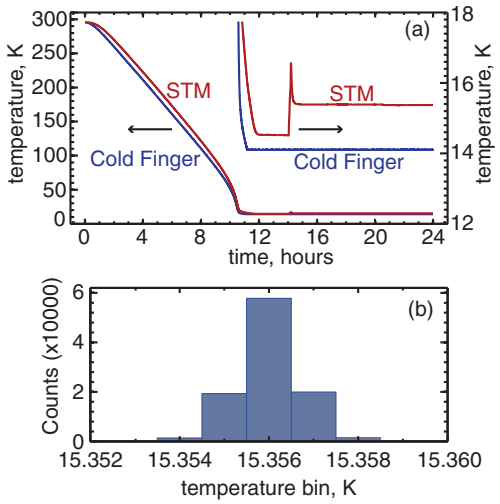

FIG. 4. (a) Typical cool down curves showing temperatures measured at the STM and at the Cold Finger. The two curves in the upper right corner show the variation of the temperatures after unclamping of the STM (seen as a spike in the top curve). (b) Histogram showing typical variations of the STM temperature when the temperature stabilization feedback mechanism is engaged. Each count corresponds to an individual reading of the temperature by the controller electronics.

B. Atomic resolution

The imaging capabilities of the new STM under cryogenic conditions were tested on several different samples with different surface structures. Figure 5(a) shows a topography scan of a Au(111) surface (acquired at ~16 K), which displays a clear hexagonal atomic pattern characteristic of the Au(111) surface,[22] with no identifiable features attributable to the CCC noise. Figure 5(c), a cross-section of topography from Fig. 5(a), shows well-defined atomic corrugation of ~10 pm. Another example of atomic-scale resolution, Fig. 5(b), shows a topography scan of a NaCl(100) monolayer film thermally deposited on the Au(111) surface (image acquired at ~16 K). Figure 5(b) shows a square lattice with a lattice constant of 0.39 nm, as expected for the NaCl(100) lattice. Similarly to Fig. 5(a), no identifiable features attributable to the CCC noise are present in the image. Figure 5(d), a cross-section of topography from Fig. 5(b), shows well-defined atomic corrugation of ~10 pm, suggesting that the CCC noise is significantly less than this number. Atomic-resolution images were also obtained on single-walled carbon nanotubes deposited on the Au(111) surface, with one example shown in Fig. 5(e).

C. Noise analysis

To quantify the noise generated by the CCC more directly, with the STM operating at 16 K, we measured the tunneling current as a function of time (Fig. 6(a)) after turning off the z-piezo feedback, thus allowing the tip-sample distance Z to be modulated by the external mechanical/acoustical noise. The tunneling current in Fig. 6 clearly shows periodic spikes with a period of ~0.42 s, matching that expected for the fundamental frequency of the CCC (2.4 Hz). The typical amplitude of each spike is on the scale of ~16 pA, a ~4%

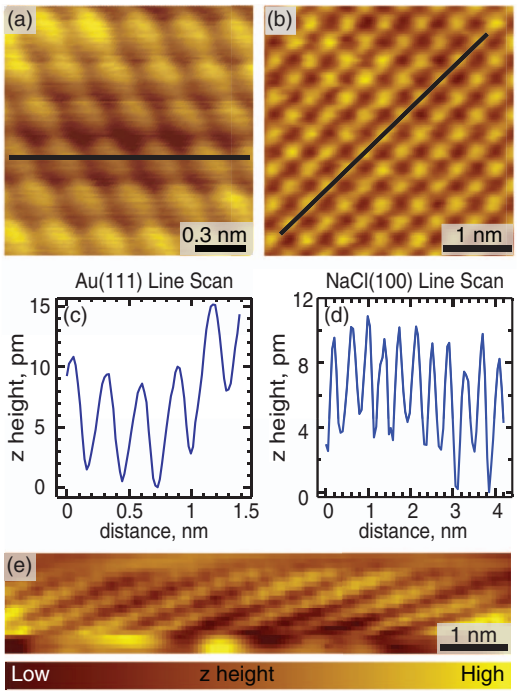

FIG. 5. Atomic-resolution images acquired with the new STM. (a) Topography scan showing atomic resolution of a reconstructed Au(111) surface [set point: 50mV, 50 pA]. The bright peaks represent the Au atoms. The atomic corrugation was enhanced by an adsorbate on the STM tip. (b) Topography scan of a monolayer of NaCl(100) thermally evaporated on the Au(111) surface [set point: 1.50 V, 10.0 pA]. The bright peaks represent the Cl atoms. (c) Cross-section of topography from (a) taken along the black line shown in (a). (d) Cross-section of topography from (b) taken along the black line shown in (b). (e) Atomically resolved surface of a single-wall carbon nanotube [set point: 1.50 V, 5.0 pA].

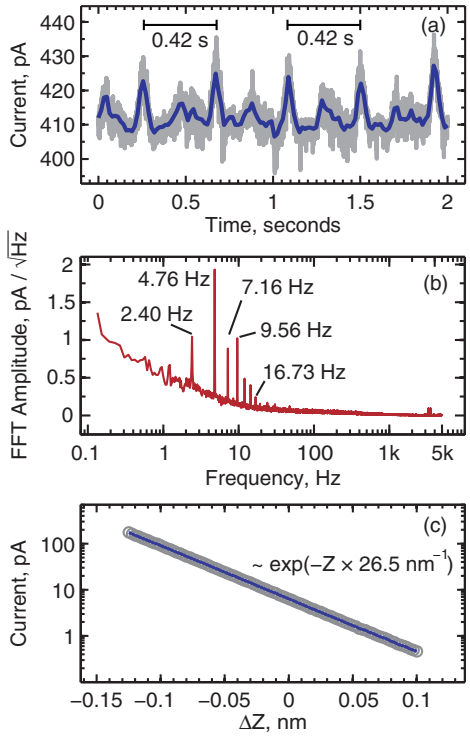

FIG. 6. Quantification of the CCC-induced noise in the tunneling current. (a) Tunneling current as a function of time (gray curve, z-feedback turned off), with the CCC operating at 15 K. To more clearly show the mechanical component of the CCC-noise, the current was measured with a low-pass filter with a corner frequency of 250 Hz. Despite the spike-like shape of the CCC-noise, only a limited number of higher harmonics with frequencies up to ~19 Hz are distinguishable in the Fourier spectra of the tunneling current [Fig. 6(b)], which means that the CCC mechanical noise in Fig. 6(a) is not affected by the 250 Hz filter. The dark blue curve, obtained by numerical filtering of the tunneling current data, serves as a guide to the eye. (b) Fourier transform of the tunneling current showing the overtones of the CCC fundamental frequency (~2.4 Hz) at 4.76, 7.16, 9.56 and 16.73 Hz. (c) Exponential dependence of the tunneling current on Z. Tunneling set point used: 1 V, 410 pA.

correction to the total current. We estimate the corresponding noise-induced variation in Z by measuring the relationship between the tunneling current and Z at a fixed bias voltage (Fig. 6(c)). Using the found exponential relation, we find that a ~4% variation in current should produce a 1.5 pm variation in Z. This is a small number as compared to the atomic corrugations observed in Fig. 5, explaining the lack of CCC-induced noise features in our STM images.

D. Scanning tunneling spectroscopy

STS measurements were carried out using the lock-in technique, with the modulation frequency typically in the range from 500 to 1000 Hz. With typical lock-in time constants being on the scale of at least a few hundred milliseconds, the lock-in signal is not expected to be very sensitive to the small current noise generated by the CCC, due to its low frequency of 2.4 Hz, even though higher harmonics (up to ~19 Hz) are distinguishable in the Fourier spectra of the tunneling current (Fig. 6(b)). This expectation is universally corroborated by the STS spectra measured for several nanoscale and molecular materials including: carbon nanotubes, PbS and CdSe quantum dots, and oligothiophene molecules. As a representative example of STS measurements, here we show a spectrum of a carbon nanotube deposited on the Au(111) surface (Fig. 7). The STS spectrum of the nanotube clearly

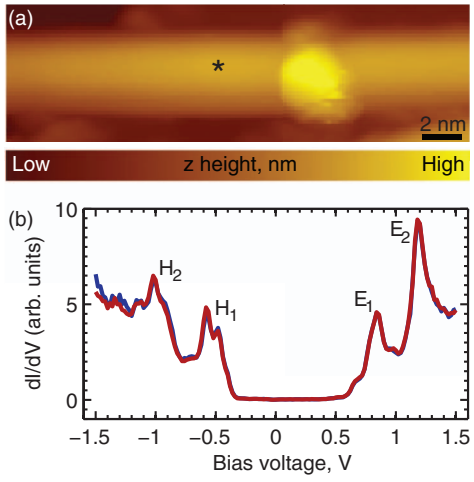

FIG. 7. STS spectroscopy of a single-wall carbon nanotube. (a) STM image of the nanotube. (b) Two STS spectra measured in one sweep from −1.5 V to 1.5 V (red curve) and back to −1.5 V (blue curve). The spectra were measured in the location shown by an asterisk in (a). The peaks observed in (b) are identified as Van Hove singularities associated with the valence (peak H_1) and conduction (peak E_1) bands. Higher order bands H_2 and E_2 are also observed. The STS spectra were obtained by measuring differential conductance, dI/dV, using the lock-in technique with a modulation of 20 mV. Tunneling set point: 1.5 V, 0.1 nA. Acquisition time: 2 min per spectrum.

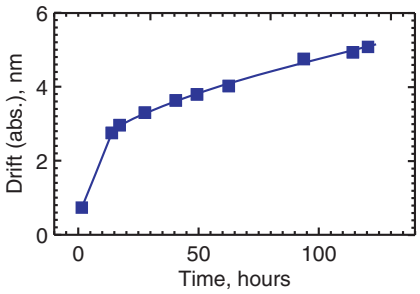

FIG. 8. X-Y spatial drift as a function of time. The drift was calculated by comparing STM images of the same area.

shows the first and second Van Hove singularities visible both in the valence and conduction bands, with the bandgap being ~1.3 eV. Both forward and backward sweeps are presented showing reproducibility of the data.

E. Spatial drift analysis

One of the critical specifications of a spectroscopic STM is its intrinsic rate of spatial drift: many types of STM-based spectroscopic measurements require extended data acquisition, which makes results sensitive to spatial drift on the atomic scale. Examples of such spectroscopic measurements are Inelastic Tunneling Spectroscopy,[23] Scanning Tunneling Luminescence,[15] or simply detailed mapping of STS spectra of individual molecules. To quantify the typical rates of spatial drift in our STM, we compared STM images taken over the course of 120 h (images not shown). Figure 8 shows that the lateral drift (caused primarily by the piezo creep after moving by 40 nm into a new area) slows down dramatically over the period of the first 15 h, and reaches a small steady drift rate of 0.18 Å/h after the first 30 h.

IV. CONCLUSION

The atomically resolved data collected using the new STM demonstrate, for the first time, the feasibility of combining an ultra-high vacuum STM instrument with a closed-cycle cryostat for achieving near-liquid helium temperatures necessary for the optimal performance of scanning tunneling spectroscopy. The use of a closed-cycle cryostat eliminates costs associated with liquid-helium, and removes limitation on the durations of individual experiments. The quality of the collected data shows that the new STM is functionally equivalent to the existing high-performance cryogenic STM systems. Additionally, the STM spatial drift rate may be further reduced by using active stabilization of the scanner temperature with a feedback-controlled heater. The combination of a virtually unlimited experiment duration and reduced spatial drift afforded by the new design will enable significantly more detailed spectroscopic investigations of samples that require extended characterization times. This, for example, includes a wide variety of samples important for nanoscale materials science, because nanoscale materials (quantum dots, carbon nanotubes, nanowires, thin films, etc.) often exhibit pronounced structural or compositional inhomogeneities.

ACKNOWLEDGMENTS

We would like to thank Jeffrey Garman, Kris Johnson, and John Boosinger of the University of Oregon machine shop for their expert machining and help in the construction process. We thank Dr. Ryan Murdick (RHK Technology) for his contribution to the construction of the STM scanner. We thank Advanced Research Systems for their help during the troubleshooting stage of the project. This work was supported by the U.S. National Science Foundation under Grant No. DMR-0960211. Additional funding was provided by the Oregon Nanoscience and Micro-technologies Institute under Grant No. 16716.

[1]C. J. Chen, *Introduction to Scanning Tunneling Microscopy* (Oxford University Press, New York, 2008).
[2]S. Behler, M. K. Rose, J. C. Dunphy, D. F. Ogletree, M. Salmeron, and C. Chapelier, Rev. Sci. Instrum. **68**, 2479 (1997).
[3]B. C. Stipe, M. A. Rezaei, and W. Ho, Rev. Sci. Instrum. **70**, 137 (1999).
[4]E. T. Foley, N. L. Yoder, N. P. Guisinger, and M. C. Hersam, Rev. Sci. Instrum. **75**, 5280 (2004).
[5]G. Meyer, Rev. Sci. Instrum. **67**, 2960 (1996).
[6]S. H. Pan, E. W. Hudson, and J. C. Davis, Rev. Sci. Instrum. **70**, 1459 (1999).
[7]B. J. Albers, M. Liebmann, T. C. Schwendemann, M. Z. Baykara, M. Heyde, M. Salmeron, E. I. Altman, and U. D. Schwarz, Rev. Sci. Instrum. **79**, 033704 (2008).
[8]S. Zhang, "United States extends life of helium reserve: Congress moves to head off shortages, but US researchers still face ballooning prices," Nature News, 26 September 2013.
[9]CS202PF-X20B Cryostat from Advanced Research Systems, Inc., Macungie, PA.
[10]T. Tomaru, T. Suzuki, T. Haruyama, T. Shintomi, A. Yamamoto, T. Koyama, and R. Li, Cryogenics **44**, 309 (2004).
[11]Cryostat noise specifications are available from Advanced Research Systems, Inc., Macungie, PA.
[12]RHK Technology, Inc., Troy, MI.
[13]H. J. Hug, B. Stiefel, P. J. A. van Schendel, A. Moser, S. Martin, and H. J. Guntherodt, Rev. Sci. Instrum. **70**, 3625 (1999).
[14]X. H. Qiu, G. V. Nazin, and W. Ho, Science **299**, 542 (2003).
[15]C. Chen, P. Chu, C. A. Bobisch, D. L. Mills, and W. Ho, Phys. Rev. Lett. **105**, 217402 (2010).
[16]G. V. Nazin, X. H. Qiu, and W. Ho, Phys. Rev. Lett. **90**, 216110 (2003).
[17]S. W. Wu, G. V. Nazin, and W. Ho, Phys. Rev. B **77**, 205430 (2008).
[18]Shapal, Precision Ceramics, Birmingham, England.
[19]P. M. Albrecht and J. W. Lyding, Appl. Phys. Lett. **83**, 5029 (2003).
[20]Series 99 Pulse Valve, Parker Hannifin Corporation, Hollis, NH.
[21]Z. Q. Wei, S. Guo, and S. A. Kandel, J. Phys. Chem. B **110**, 21846 (2006).
[22]J. V. Barth, H. Brune, G. Ertl, and R. J. Behm, Phys. Rev. B **42**, 9307 (1990).
[23]B. C. Stipe, M. A. Rezaei, and W. Ho, Science **280**, 1732 (1998).